

Journal of Geophysical Research: Atmospheres

RESEARCH ARTICLE

10.1002/2014JD022659

Key Points:

- A coupled climate model has four stable states; one state has tropical sea ice
- Tropical ice caps are stabilized by intense wind-driven ocean heat transport
- Cold climates are very sensitive to spatial structure of ocean heat transport

Correspondence to:B. E. J. Rose,
brose@albany.edu**Citation:**Rose, B. E. J. (2015), Stable "Waterbelt" climates controlled by tropical ocean heat transport: A nonlinear coupled climate mechanism of relevance to Snowball Earth, *J. Geophys. Res. Atmos.*, 120, doi:10.1002/2014JD022659.

Received 1 OCT 2014

Accepted 23 JAN 2015

Accepted article online 28 JAN 2015

Stable "Waterbelt" climates controlled by tropical ocean heat transport: A nonlinear coupled climate mechanism of relevance to Snowball Earth

Brian E. J. Rose¹¹Department of Atmospheric and Environmental Sciences, University at Albany, Albany, New York, USA

Abstract Ongoing controversy about Neoproterozoic Snowball Earth events motivates a theoretical study of stability and hysteresis properties of very cold climates. A coupled atmosphere-ocean-sea ice general circulation model (GCM) has four stable equilibria ranging from 0% to 100% ice cover, including a "Waterbelt" state with tropical sea ice. All four states are found at present-day insolation and greenhouse gas levels and with two idealized ocean basin configurations. The Waterbelt is stabilized against albedo feedback by intense but narrow wind-driven ocean overturning cells that deliver roughly 100 W m^{-2} heating to the ice edges. This requires three-way feedback between winds, ocean circulation, and ice extent in which circulation is shifted equatorward, following the baroclinicity at the ice margins. The thermocline is much shallower and outcrops in the tropics. Sea ice is snow-covered everywhere and has a minuscule seasonal cycle. The Waterbelt state spans a 46 W m^{-2} range in solar constant, has a significant hysteresis, and permits near-freezing equatorial surface temperatures. Additional context is provided by a slab ocean GCM and a diffusive energy balance model, both with prescribed ocean heat transport (OHT). Unlike the fully coupled model, these support no more than one stable ice margin, the position of which is slaved to regions of rapid poleward decrease in OHT convergence. Wide ranges of different climates (including the stable Waterbelt) are found by varying the magnitude and spatial structure of OHT in both models. Some thermodynamic arguments for the sensitivity of climate, and ice extent to OHT are presented.

1. Introduction

The high shortwave reflectivity of surface ice and snow relative to open water and vegetated surfaces introduces a profound nonlinearity into the climate system. Runaway positive albedo feedback for large ice caps was first discovered as a mathematical principle in simple but physically plausible climate models [Budyko, 1969; Sellers, 1969]. These simple models predict that multiple stable climate states are possible for a given radiative forcing. In particular, a fully ice-covered planet would be stable at present-day insolation and greenhouse gas levels. See North *et al.* [1981] for a comprehensive review of early work. The stability of the ice-covered Earth has been confirmed in a number of modern comprehensive climate models [e.g., Marotzke and Botzet, 2007; Ferreira *et al.*, 2011; Voigt *et al.*, 2011; Yang *et al.*, 2012a].

The Snowball Earth hypothesis [Kirschvink, 1992; Hoffman *et al.*, 1998] proposes that the global oceans froze over during the widespread glaciations of the Late Neoproterozoic Era, linking the mathematical theory of runaway albedo feedback to the geological record. The simple theories demand a very strong radiative forcing to initiate melting of the tropical oceans in order to exit the fully glaciated state, which is thought to have been provided by volcanic outgassing of CO₂ in the absence of significant chemical weathering. Indeed, the post-glacial cap carbonate sequences and other geochemical evidence strongly suggest that Snowball terminations involved a climatic bifurcation and rapid transition to a much warmer climate state (see review by Pierrehumbert *et al.* [2011]), consistent with the simplest albedo-feedback models.

A major challenge to this "Hard Snowball" scenario (meaning 100% ice cover) is the lack of biological evidence for major extinctions of photosynthetic organisms. One possibility is that tropical sea ice coverage was sufficiently thin and transparent to allow photosynthesis to continue under the ice [McKay, 2000; Pollard and Kasting, 2005]. However, the leading hypothesis is that sea ice would grow to a thickness of order 1 km in a Hard Snowball scenario, limited by the geothermal heat flux into the oceans [e.g., Ashkenazy *et al.*, 2013], necessitating other types of biological refugia [e.g., Campbell *et al.*, 2011; Tziperman *et al.*, 2012]. Alternatively, large expanses of tropical ocean may have remained unfrozen (and thus biologically

productive) during Snowball glaciations. This view is supported by recent evidence of Snowball-era fluvial deposits and periglacial features consistent with surface temperatures near the freezing point [Ewing et al., 2014]. A number of climate model studies have revealed stable climates with sea ice margins at or equatorward of 30° latitude [e.g., Hyde et al., 2000; Poulsen et al., 2001; Donnadieu et al., 2004; Yang et al., 2012a]. Pierrehumbert et al. [2011] introduced the term “Waterbelt” to describe such climate states. These studies have typically used some combination of reduced solar luminosity, reduced atmospheric CO₂, and a high-albedo tropical supercontinent to investigate Snowball initiation under climatic boundary conditions appropriate to the Neoproterozoic. Tropical land surfaces in Waterbelt climate simulations are typically cold enough to support low-latitude glaciation [e.g., Hyde et al., 2000], suggesting that Snowball Earth ice sheets could have existed alongside open tropical ocean. However, few of these studies have proposed a bifurcation mechanism for transitions out of the Waterbelt state. A notable exception is the so-called “Jormungand” bare sea ice albedo mechanism first elucidated by Abbot et al. [2011]; we will address this in the discussion section.

In this study, we use a coupled atmosphere-ocean-sea ice general circulation model (GCM) to investigate a stable Waterbelt-type climate state and show that it does in fact have a significant bifurcation and hysteresis associated with it. The physical mechanism is entirely novel and involves a very active role for the wind-driven tropical ocean circulation and associated ocean heat transport (OHT). Our aim is not to solve all the above Neoproterozoic climatic riddles but simply to explore the possibility of multiple equilibria and hysteresis in the climate system, using the coupled model to quantify the relevant physical mechanisms. We will also use some reduced-order models to better understand the sensitivity of the global climate system to the shape and magnitude of low-latitude OHT.

OHT out of the tropics has been shown to play an important role in stabilizing Waterbelt climates in a number of different Snowball-inspired model studies [e.g., Poulsen et al., 2001; Donnadieu et al., 2004; Poulsen and Jacob, 2004; Yang et al., 2012b, 2012c; Voigt and Abbot, 2012]. Rose and Marshall [2009] argued on the basis of highly idealized yet physically based models of wind-driven OHT that multiple stable configurations of sea ice cover and ocean circulation might be possible, even at present-day radiative forcing. Ferreira et al. [2011] subsequently found multiple equilibria in a coupled atmosphere-ocean-sea ice GCM with idealized ocean basin geometry. For identical insolation and greenhouse gas levels, three stable equilibria were found: a Warm state with polar oceans near freezing but largely ice free, a Cold state with large sea ice caps extending into the midlatitudes, and a fully ice-covered Snowball state. These multiple states arise in the coupled GCM from integrations differing in initial condition but otherwise using identical parameters.

One of the key points of this paper is that the results of Ferreira et al. [2011] were incomplete. A new, fourth stable equilibrium has been found in two different configurations of the coupled model. The fourth state, which we refer to here as the Waterbelt, has sea ice extending into the tropics. The four equilibria are illustrated in Figure 1, showing SST and sea ice distributions. We can rank the four states in decreasing global mean temperature as Warm, Cold, Waterbelt, and Snowball.

The coupled GCM, the new Waterbelt simulation, and its hysteresis are described in detail in section 2. Section 3 uses uncoupled slab ocean GCM experiments with prescribed OHT to investigate how the number and type of climatic equilibrium depends on the magnitude and spatial structure of OHT. Section 4 uses a much simpler diffusive energy balance model with prescribed OHT and simple sea ice thermodynamics to build a deeper understanding of the unique role played by the oceans in stabilizing cold Waterbelt states. In section 5, we discuss the results (and their possible relevance to Snowball Earth) in the context of previous literature and conclude.

2. A Stable Waterbelt in a Coupled Model Simulation

2.1. Coupled Model Description

The numerical model is the coupled MITgcm [Marshall et al., 1997, 2004] in “aquaplanet” configuration. The coupled model setup is identical to that used by Ferreira et al. [2011] and Rose et al. [2013]. Atmosphere, ocean, and sea ice components use the same cubed-sphere grid at coarse C24 resolution (3.75° at the equator), ensuring as much fidelity in model dynamics at the poles as elsewhere. The ocean component is a primitive equation non-eddy-resolving model, using the rescaled height coordinate z^* [Adcroft and Campin, 2004] with 15 levels and a flat bottom at 3 km depth (chosen to approximate present-day ocean volume

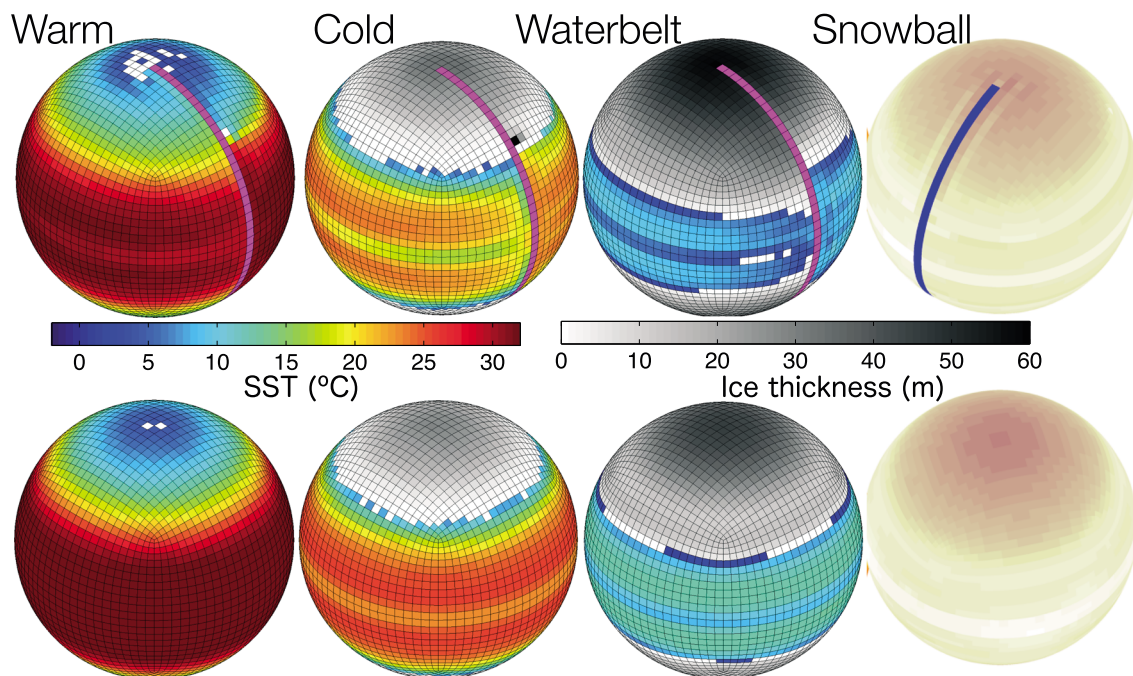


Figure 1. Multiple equilibria in *Ridge* and *Aqua*. The “Waterbelt” state with tropical sea ice edge is found here, in addition to the three states reported by Ferreira et al. [2011]. All simulations are fully equilibrated with no drift in temperature and ice thickness (the Snowball state has a very small drift in ice thickness due to the absence of geothermal heating).

and thus total heat capacity). Subgrid scale parameterizations include advective mesoscale eddy transport [Gent and McWilliams, 1990], isopycnal diffusion [Redi, 1982], and vertical convective adjustment [Klinger et al., 1996]. Vertical diffusivity is uniform at $3 \times 10^{-5} \text{ m}^2 \text{ s}^{-1}$, and we use a nonlinear equation of state [Jackett and McDougall, 1995].

The atmosphere is a five-level primitive equation model with moist physics based on SPEEDY [Molteni, 2003]. These include four-band long and shortwave radiation schemes with interactive water vapor channels, diagnostic clouds, a boundary layer scheme, and mass-flux moist convection scheme. Vertical pressure coordinates are used, with one level in the boundary layer, three in the free troposphere, and one in the stratosphere. Details about these parameterizations (substantially cruder than used in IPCC-class models) are given in Rose and Ferreira [2013]. Present-day atmospheric CO₂ is prescribed. Insolation varies seasonally (23.5° obliquity, zero eccentricity), but there is no diurnal cycle.

The sea ice component is a three-layer thermodynamic model based on Winton [2000] (two layers of ice plus surface snow cover). The model allows for partially ice-covered grid cells; prognostic variables include ice fraction, snow and ice thickness, and ice enthalpy accounting for brine pockets with an energy-conserving formulation. Ice surface albedo depends on ice thickness, temperature, snow depth, and age; for *Ridge*, it ranges between a minimum of 0.25 for thin, bare ice to a maximum of 0.8 for a thick, cold layer of fresh snow. Slightly different values are used in *Aqua*; all details are given in Ferreira et al. [2011]. A diffusion of ice thickness is used as a proxy for ice dynamics, representing the net large-scale export of ice from the polar regions. Due to the use of the z^* coordinate, the model does not require artificial limits on sea ice thickness to avoid the drying out of the ocean cells. This enables long integrations with machine-level conservation of heat, water, and salt and without numerical drift [Campin et al., 2008], and is a considerable asset for the study of very cold climates in which the sea ice becomes very thick.

Two different ocean configurations are used, as illustrated in Figure 1. *Aqua* is a pure aquaplanet with zonally unbounded ocean at all latitudes. *Ridge* has a thin pole-to-pole continent confining the ocean into a single global-scale basin and giving rise to gyre circulations. See Ferreira et al. [2011] and Rose et al. [2013] for further discussion.

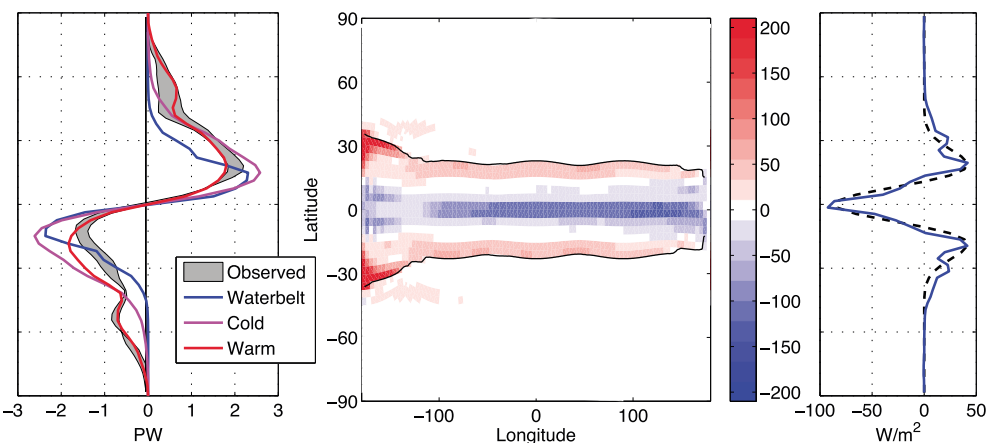


Figure 2. Ocean heat transport and convergence. (left) OHT (in PW) from the three non-Snowball states of *Ridge* shown in Figure 1. The grey shading spans two different observational estimates of present-day OHT [Trenberth and Caron, 2001]. (center) Spatial map of OHT convergence (W m^{-2}) in the Waterbelt *Ridge* simulation, with the ice edge indicated by the black contours. This shows the zonal asymmetries associated with the subtropical gyre circulation. (right) zonal average convergence in Waterbelt (blue line). The dashed black line is the convergence estimated from equation (1) with $N = 14$ and 2.5 PW amplitude.

2.2. Climatology of the Waterbelt

Figure 1 shows four equilibrium climates in each configuration. These simulations differ *only* in initial conditions, and use identical parameters. Thus, the Warm, Cold, Waterbelt, and Snowball states are all consistent with present-day insolation and greenhouse gas levels in this model. The Waterbelt states were discovered in transient experiments with time-varying solar constant [Rose *et al.*, 2013], which are described below.

The Waterbelt states are substantially colder than the Cold state reported in Ferreira *et al.* [2011]. SST does not exceed 12°C and 14°C in *Ridge* and *Aqua*, respectively. The sea ice edge is around 29° latitude in *Aqua*. *Ridge* has much more zonal asymmetry in both SST and ice cover due to the subtropical gyre circulation; the ice edge ranges from around 35° on the western edge of the basin to near the equator on the eastern edge (Figure 2), with an effective ice latitude [Rose *et al.*, 2013] of 24°. Wind-driven upwelling maintains very cold SSTs along the equator—cold enough to support some equatorial sea ice on the eastern side of the basin in *Ridge*.

2.2.1. Ocean Heat Transport

Previous works have shown that convergence of OHT near the ice edge plays a key role in the stabilization of cold, icy climates [Rose and Marshall, 2009; Ferreira *et al.*, 2011; Rose *et al.*, 2013]. We therefore expect that the transition from Cold to Waterbelt climate requires a reorganization of the ocean circulation to deliver heat over a more meridionally restricted range of latitudes. To confirm this, we plot the simulated OHT and its convergence in Figure 2. Figure 2 (left) shows OHT in the Warm, Cold, and Waterbelt states of *Ridge*, along with an estimate of the present-day OHT on Earth. All three model configurations, as well as the observations, feature substantial poleward heat transport out of the deep tropics in both hemispheres. However, the meridional scale of the OHT in the Waterbelt state (i.e., the range of latitudes over which the convergence occurs) is much smaller than either the observations or the other states of the coupled model. The Waterbelt ocean is carrying large amounts of energy (about 2.4 PW in both hemispheres) over short distances.

Figure 2 (center) shows the spatial structure of the annual mean heat flux out of the ocean in the Waterbelt (i.e., the OHT convergence). The sea ice margin is also shown in the black, revealing the intimate relationship between sea ice and the heating from the ocean [Rose *et al.*, 2013]. The heat flux is strongly positive at the equatorward edge of the sea ice and drops rapidly to zero poleward of the ice edge. Open water extends poleward past 30° latitude along the western boundary of the ocean basin and is associated with maximum heat fluxes of about 200 W m^{-2} , which are sustained by the western boundary currents associated with the subtropical gyre circulation. In the zonal average, the heat flux out of the ocean peaks at about 40 W m^{-2} and occurs around 20° latitude, just equatorward of the zonal average ice edge. The dashed line shows an analytical approximation to the zonal mean heat flux introduced in section 3.

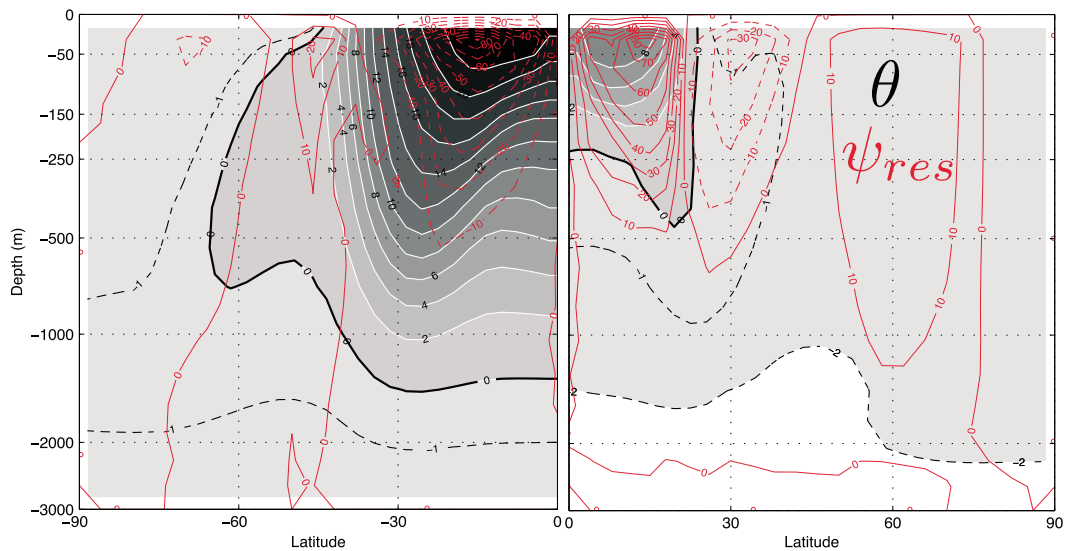


Figure 3. Zonally averaged potential temperature (gray shading, in °C) and residual mean overturning mass streamfunction (red contours, in Sv) in the ocean for the (left) Cold and (right) Waterbelt states of *Ridge*. Only one hemisphere is shown in each case. Plotted with a logarithmically stretched depth axis to highlight upper ocean structure.

2.2.2. Ocean Overturning Circulation

In Figure 3, we compare the Cold and Waterbelt states of the ocean in *Ridge*. These plots show cross sections of the zonal average potential temperature θ and residual mean meridional overturning streamfunction ψ_{res} . Only one hemisphere is plotted as the climates are all symmetric about the equator. The vast majority of the Waterbelt ocean is below 0°C and nearly isothermal. There is a very shallow tropical thermocline that outcrops abruptly at the latitude of the sea ice edge. The most vigorous circulation is a small but intense wind-driven subtropical overturning cell that operates over the region of strong temperature gradients associated with the shallow thermocline. This circulation is largely responsible for the 2.4 PW poleward heat transport out of the deep tropics.

The subtropical overturning cell is driven by the spatial pattern of surface winds (tropical easterlies and midlatitude westerlies) and is a very robust feature of the circulation [Klinger and Marotzke, 2000; Ferreira et al., 2011]. The Cold and Waterbelt states of *Ridge* feature very similar wind-driven mass fluxes (about 80 Sv) but quite different meridional extents. The downwelling branch of the overturning cell in Waterbelt occurs in a narrow region of nearly vertical isotherms near 20° latitude and is associated with significant convection at the sea ice margin [see Rose et al., 2013]. By contrast, the downwelling branch in the Cold state occurs over a diffuse region between 20 and 40° latitude associated with subduction within the subtropical gyre. The narrow meridional scale of the OHT in Waterbelt is a consequence of the narrow scale of the subtropical overturning.

2.2.3. Wind Stress

Figure 4 compares the surface wind forcing from the Cold and Waterbelt states of *Ridge* with an observed climatology [Trenberth et al., 1989]. We plot the zonal mean zonal wind stress τ_x as well as the Ekman pumping $w_{ek} = \nabla \times (\vec{\tau}/(\rho_0 f))$ (not plotted within 10° of the equator, where w_{ek} is poorly defined). The simulations differ substantially from the observations, particularly in the location of the midlatitude westerlies.

Relative to the observations, the positions of the midlatitude westerly and tropical easterly τ_x maxima are shifted equatorward in Cold and even more so in Waterbelt. The equatorward shift is even more apparent in the plots of w_{ek} . The peak downward Ekman pumping in the Waterbelt is a factor of 2 larger than found in the Cold state or the observations and is shifted equatorward by about 10° latitude. The spatial map of w_{ek} for Waterbelt in Figure 4 shows that the peak Ekman pumping is roughly zonally symmetric and aligned with the sea ice edge (except for the asymmetric region of open water on the western boundary). The peak w_{ek} is roughly equivalent to the zero wind stress line separating the band of tropical easterlies from midlatitude westerlies. In Waterbelt, the wind systems are all displaced closer to the equator. The winds are thus acting strongly to pump fluid downward near the ice edge and setting the narrow, intense overturning circulation that is in turn responsible for the stability of the ice edge.

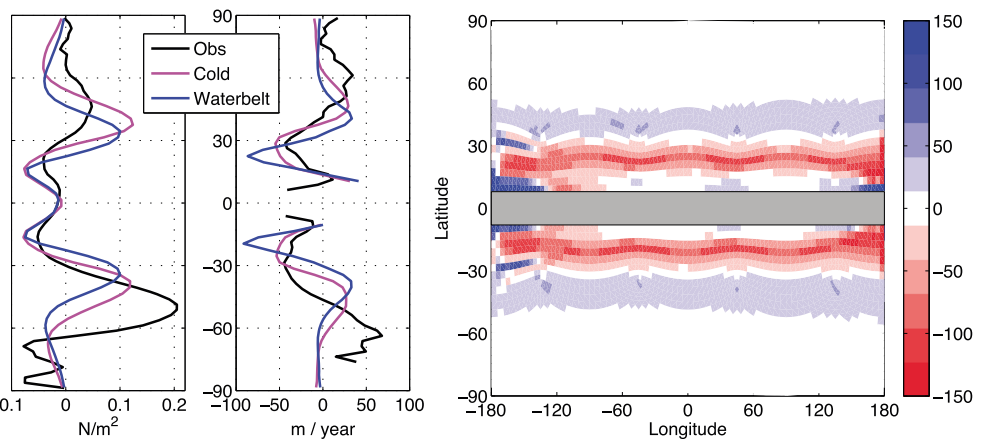


Figure 4. Wind forcing on the ocean. (left) Zonal stress τ_x (zonal, annual mean). (center) Ekman pumping $w_{ek} = \nabla \times (\tau / (\rho_0 f))$. These plots compare the Waterbelt Ridge (blue) to the Cold Ridge (magenta) and observations [Trenberth et al., 1989]. (right) Spatial map of Ekman pumping in the Waterbelt Ridge. Negative values (red) indicate downward Ekman velocity (i.e., pumping). Units are $m yr^{-1}$.

2.2.4. Atmospheric Circulation

Figure 5 shows atmospheric cross-sections of the zonal-mean zonal winds and potential temperature, again comparing the Cold and Waterbelt states of *Ridge*. This figure reveals that the equatorward shift in the winds in Waterbelt is not limited to the surface. The entire westerly jet structure is shifted equatorward relative to the Cold state. In both cases, the near-surface temperature gradients are largest in the vicinity of the sea ice edge (45° and 25° latitude, respectively, for Cold and Waterbelt). We surmise that the equatorward shift of the surface wind systems is intimately connected to the equatorward shift of the zones of strong baroclinicity around the sea ice margin.

2.2.5. Summary

Four qualitatively different climates are found in a coupled ocean-atmosphere-sea ice GCM. The new state, which we have called the Waterbelt, features large sea ice caps covering more than half the surface of the planet. This state appears to be stabilized by intense ocean heat transport by tropical overturning cells. This circulation is driven by a pattern of surface wind forcing that is shifted equatorward relative to its usual position. The wind shift appears to be tightly coupled to the strong baroclinicity associated with the tropical ice edge. Thus the Waterbelt state depends on three-way interactions between the ocean, sea ice, and atmosphere.

2.3. Hysteresis in Response to Radiative Forcing

Rose et al. [2013] reported on hysteresis and abrupt climate changes in *Ridge* and *Aqua* in response to slow imposed variations in solar constant. The previous work dealt only with transitions between the Warm and Cold states. We have carried out additional long simulations with slightly larger-amplitude variations in solar constant to illustrate transitions in and out of the new Waterbelt state. The experimental setup is identical to Rose et al. [2013]. We initialize the coupled GCM integrations from either the Warm and Cold equilibrium state with the reference solar constant. We then impose gradual (sinusoidal) variations in solar constant over an 8000 year simulation. This long timescale is chosen in order to separate the forcing from the climate response as cleanly as possible given computational constraints. The solar constant is used as the control parameter in these experiments for convenience. We expect that analogous results would be generated by varying other forms of radiative forcing such as greenhouse gas concentration.

The results for *Ridge* are shown in Figure 6. The upper panels show the imposed solar constant variations; lower panel shows the timeseries of the ice area (plotted as an equivalent latitude [Rose et al., 2013]), with each color representing a different simulation. The red and blue curves are reproduced from Rose et al. [2013]; they show that $\pm 20 W m^{-2}$ variations in solar constant (or $\pm 5 W m^{-2}$ global mean insolation as reported by Rose et al. [2013]) are sufficient to drive transitions between the Warm and Cold states. The coupled GCM exhibits hysteresis in the sense that the climate undergoes large transitions and does not relax back to its initial equilibrium once the solar constant returns to its reference value around year

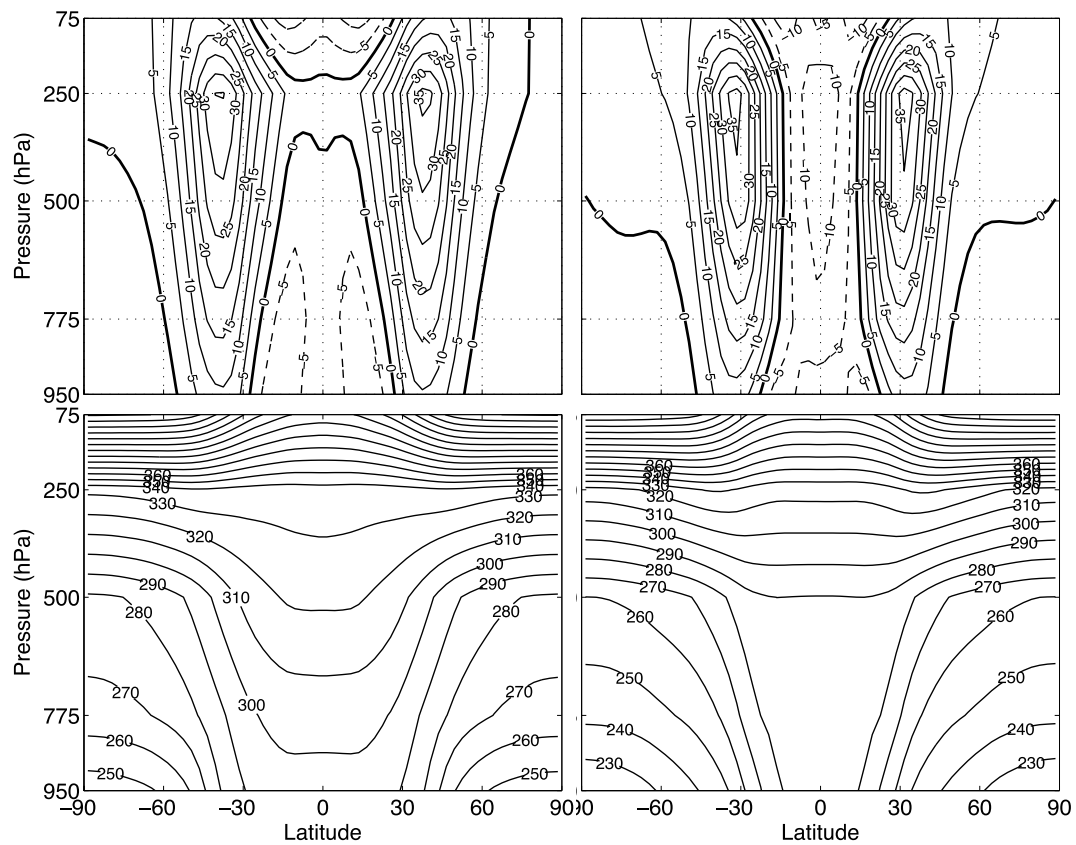


Figure 5. Zonally averaged zonal wind (upper) and potential temperature (lower) for the Cold (left) and Waterbelt (right) states of *Ridge*. For the wind, solid and dashed curves indicate westerly and easterly flow respectively, with the zero contour highlighted. Contour intervals are 5 m s^{-1} for u and 10 K for θ . The five model levels are centered at the pressures indicated on the vertical axes ($950, 775, 500, 250$, and 75 hPa); contours are interpolated smoothly between these levels.

4000. See Rose *et al.* [2013] for a detailed analysis of the role of ocean circulation in setting the pace of these transitions.

The new results are plotted in magenta and cyan in Figure 6. Here we increase the amplitude of the forcing slightly to $\pm 24 \text{ W m}^{-2}$. The impact on the simulated climate is startlingly different, revealing the existence of a qualitatively different equilibrium state in the model—the Waterbelt. For example, the magenta curve illustrates the case that begins Warm and ice-free. The initial cooling and growth of ice looks very similar to the red curve, but cooling and ice expansion is more rapid during years 2000–3000, and the ice eventually reaches the tropics and begins to stabilize. The second half of this simulation (years 4000–8000) shows that the Waterbelt is in fact more robust than the Cold state reported by Ferreira *et al.* [2011] and Rose *et al.* [2013]: the 24 W m^{-2} increase in insolation is insufficient to deglaciate the model. The black curve shows that the Waterbelt is indeed a stable equilibrium at the reference solar constant: the ice edge does not evolve over a 4000 year integration.

A large number of long equilibrium simulations with fixed parameters was used to map out the detailed bifurcation diagram for *Ridge*. All four model states in Figure 1 were used as initial conditions, and the model was run out to equilibrium with a wide variety of different solar constants. The results are plotted in Figure 7. Five bifurcations are shown here, bracketing either end of the stable ranges for Cold and Waterbelt states, and the cold end of the Warm range. The sixth bifurcation at high solar constant—the Snowball deglaciation—is not shown and has not been quantified in this model.

The Waterbelt ice edge lies between 21° and 30° equivalent latitude (64% to 50% fractional ice cover), with global mean temperatures from 250 to 260 K. It is found between 1341 and 1387 W m^{-2} solar constant. The Waterbelt states are well separated from the Cold states, which have ice lines between 40° and 50° and

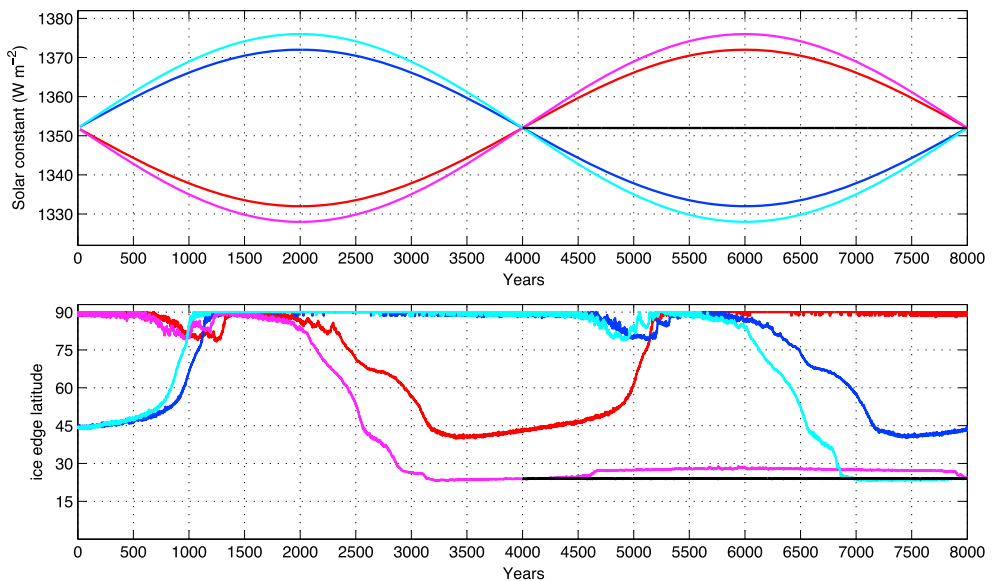


Figure 6. Evolution of the sea ice edge in long integrations of the coupled *Ridge* GCM with time-varying solar constant. The red and blue curves were described in detail by Rose et al. [2013]. This figure shows that a slight increase in the amplitude of the forcing leads to qualitatively different behavior: the model enters the Waterbelt state with subtropical sea ice. The Waterbelt state with ice edge at 24° latitude is a stable equilibrium of *Ridge* (black curve) at the reference solar constant of 1352 W m⁻² (as used by Ferreira et al. [2011] and Rose et al. [2013]), along with the Warm, Cold, and Snowball states pictured in Figure 1. Once in the Waterbelt state, the ice edge adjusts only minimally to a 35 W m⁻² increase in solar constant (magenta curve).

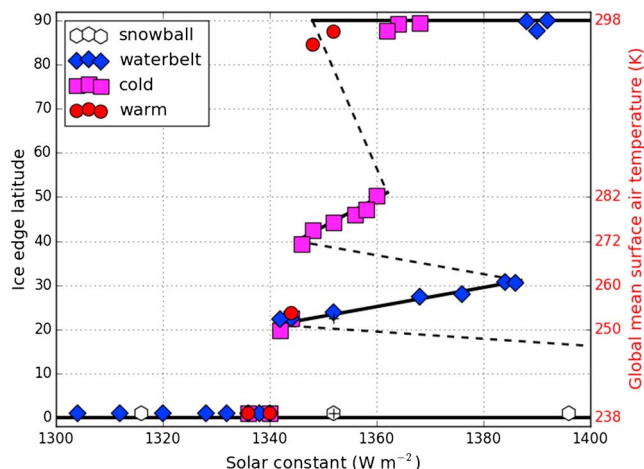


Figure 7. Bifurcation diagram for *Ridge*. Each marker represents a long equilibrium simulation of the coupled GCM with fixed parameters. The model is initialized in Warm, Cold, Waterbelt, or Snowball state as indicated by marker color. A range of solar constants is used to map out the stable branches for each model state. A stable Waterbelt is found for solar constant between 1341 and 1387 W m⁻², with ice lines ranging from 21° to 30° latitude. The red axis shows approximate global mean surface air temperature; the Waterbelt states range between 250 and 260 K. These are well separated from the Cold states, which have ice lines between 40° and 50°, and temperatures between 272 and 282 K. Black lines give a schematic sketch of the continuous bifurcation diagram of ice edge versus solar constant, with solid (dashed) lines indicating stable (unstable) branches (the critical value for Snowball deglaciation was not searched for). The two crosses at 1352 W m⁻² show a sensitivity test on the sea ice thickness diffusion coefficient: a 50% diffusivity increase leads to a stable ice expansion of 1° latitude, while a 100% increase results in a Snowball climate.

temperatures between 272 and 282 K. The Waterbelt state is substantially more stable than the Cold state. Since the modeled planetary albedo in the Waterbelt state is about 0.42, the 46 W m⁻² solar constant range is equivalent to about 7 W m⁻² in absorbed solar radiation, or roughly a quadrupling of CO₂ [Andrews et al., 2012].

The specific shape of the bifurcation diagram in Figure 7 is likely sensitive to model details. Voigt and Abbot [2012] argued that sea ice dynamics play a key role in destabilizing low-latitude ice states. The present GCM represents ice dynamics through diffusion of ice thickness. Increasing the diffusion coefficient leads to more efficient equatorward ice export and might destabilize the Waterbelt. To test this, two sensitivity tests were carried out with 50% and 100% increase in ice diffusivity respectively. Results are shown in Figure 7 (crosses at 1352 W m⁻²): a 50% increase leads to stable ice area expansion of 1° equivalent latitude, while a 100% increase results in an unstable transition to the Snowball.

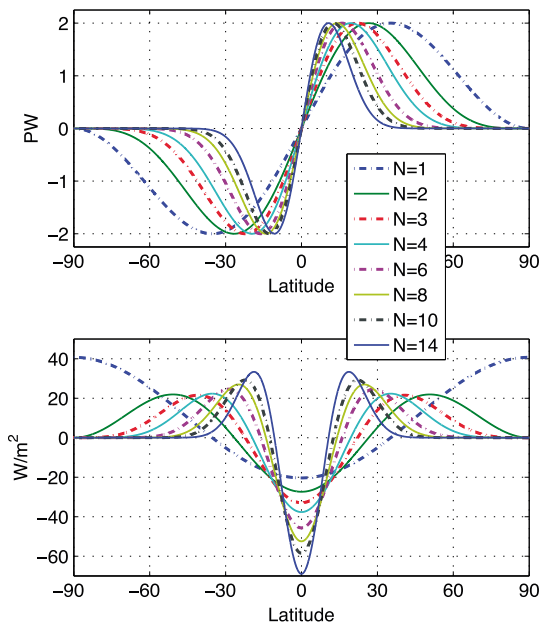


Figure 8. Ocean heat transport profiles computed from the equation (1), with amplitudes normalized to peak at 2 PW. Lower panel shows the convergences in W m^{-2} .

et al., 2013]. The atmosphere and sea ice components are identical to the full coupled GCM used in the previous section. The ocean is represented by a 60 m mixed layer with a prescribed heat source/sink term representing OHT convergence (known as a q-flux).

3.1. Setup of Prescribed Q-Flux Experiments

The OHT is prescribed to be steady in time, vary only in latitude, and anti-symmetric about the equator:

$$H_o(x) = \Psi \sin(\phi) \cos(\phi)^{2N} = \Psi x(1-x^2)^N \quad (1)$$

where $x = \sin \phi$ and ϕ is latitude, N is a positive integer, and Ψ is a constant (in units of W) setting the amplitude. This is identical to the forcing used in Rose and Ferreira [2013]. OHT and its convergence computed from equation (1) are plotted in Figure 8 for values of N ranging from 1 to 14, with Ψ scaled in each case to give a peak transport of 2 PW. N and Ψ are the two adjustable parameters in these experiments, setting (respectively) the meridional scale and amplitude of OHT. Consistent with observations, the q-flux acts to cool the deep tropics in all cases. Convergence (heating) occurs over a range of subtropical to midlatitudes, shifting equatorward for larger values of N . The forcing is conservative in all cases, acting only to redistribute energy within the ocean mixed layer.

We vary the peak amplitude between 0 and 4 PW. To sample out the multiple-branch structure of the equilibria, the model is initialized in both Warm (no ice) and Cold (ice in the midlatitudes) states (taken from Ferreira et al. [2011]) and integrated out to quasi-equilibrium in every case.

3.2. Results

Figure 9 shows the transient adjustment of the sea ice edge to equilibrium in an ensemble of simulations with the slab ocean model spanning a wide range of imposed OHT. Results are grouped into panels by the OHT scale parameter N , with different OHT amplitudes indicated by the color scale. Each curve shows the ice edge latitude in a single simulation, beginning from either Warm or Cold initial conditions. This figure reveals three qualitatively different types of climate in the slab ocean model: ice-free, large ice cap, and Snowball, depending sensitively on the amplitude and shape of the imposed OHT.

In the limit of zero OHT, sea ice rapidly expands to the equator regardless of initial conditions; thus only the Snowball climate is possible. When the imposed OHT has a broad equator-to-pole scale ($N = 1, 2$), both ice-free and Snowball climates are possible. For smaller-scale OHT ($N > 3$) of sufficiently large amplitude,

3. Climatic Impact of Ocean Heat Transport: Slab Ocean Experiments

Results in the previous section indicate that there are significant feedbacks between the ocean circulation and the rest of the climate system, and these feedbacks are instrumental in giving rise to the multiple equilibria. We have asserted that the tropical ice edge in the Waterbelt state is stabilized by OHT associated with vigorous wind-driven tropical overturning that is itself dependent on the sea ice and its effects on global wind systems. Additional insight into the climatic role of the ocean can be gained from model experiments in which feedbacks between the ocean circulation and the rest of the climate system are suppressed. In this section, we look at GCM experiments in which the OHT is prescribed and varied systematically. We seek to understand how the number and type of equilibrium climates depends on the magnitude and spatial scale of OHT.

We use a so-called slab ocean version of the numerical model [Rose and Ferreira, 2013; Rose

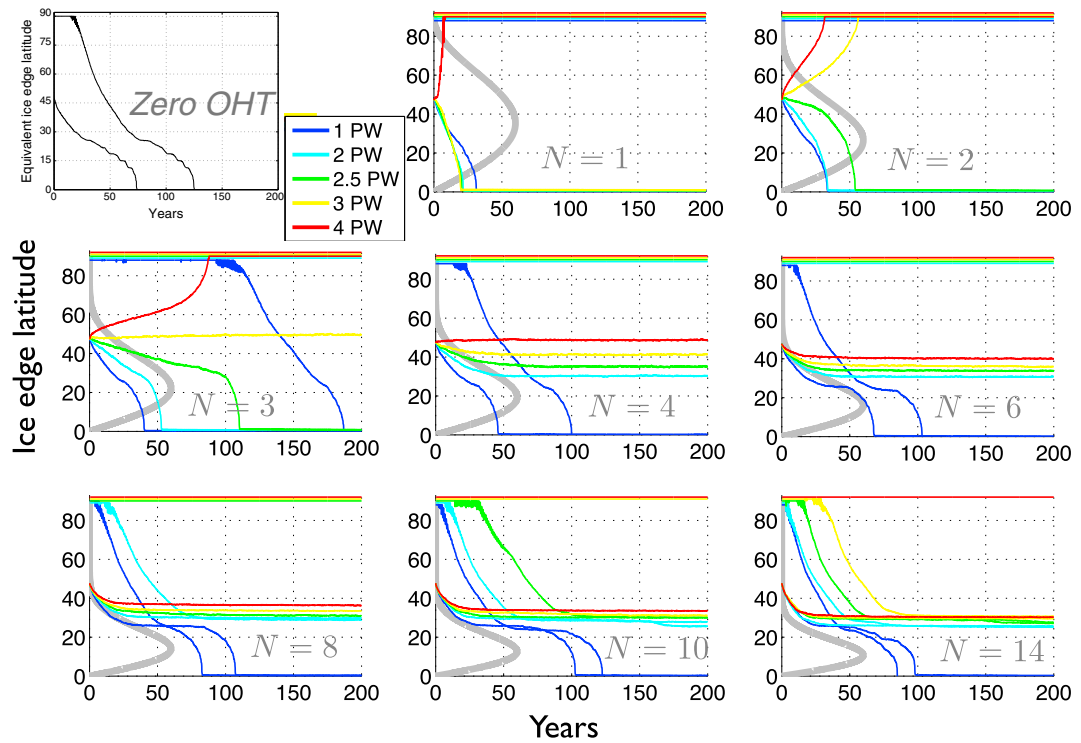


Figure 9. Ice edge latitude in slab ocean simulations. Meridional structure of prescribed OHT is sketch in thick grey curves. Colors indicate peak amplitude of prescribed OHT. Runs are initialized in two different initial conditions: no ice and ice near 45°.

three different equilibria are found (ice free, stable large ice cap, and Snowball). An important finding here is that the stable large ice cap states found in the slab ocean model exist on a continuum between the Cold and Waterbelt states of the coupled model (equilibrium ice edges between about 50° and 25° latitude), with the ice edge shifting equatorward for weaker amplitude and/or smaller-scale OHT. Figure 9 also reinforces the finding that stable Waterbelt climates with subtropical ice edges are possible in spite of strong albedo feedback. The stability of the Waterbelt depends on the capacity of the ocean to transport at least 2 PW of heat off the equator and release it to the atmosphere within a narrow band of subtropical latitudes.

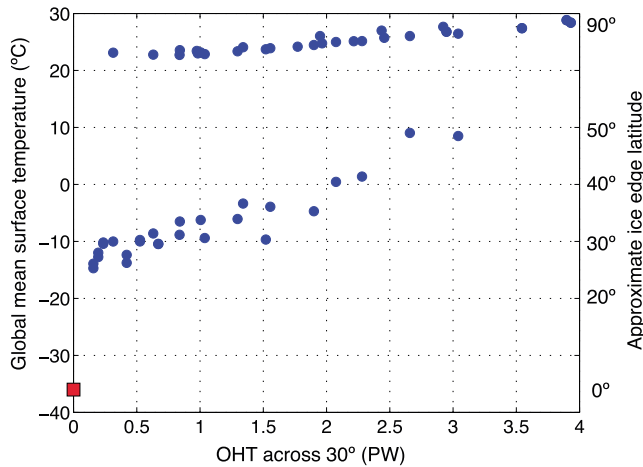


Figure 10. Global mean surface temperature \bar{T} plotted against OHT across 30°. Multiple equilibria. The right-hand axis shows the approximate ice edge latitude (which is linearly related to \bar{T} in the icy regime).

Figure 10 shows the equilibrium global mean temperature \bar{T} plotted as a function of OHT. Here the variations in amplitude and meridional scale are collapsed onto a single axis: heat flux poleward across 30° latitude. The red square shows the Snowball solution $\bar{T} = -36^\circ\text{C}$. We emphasize that the enormous range of different climates found in the slab ocean model (45°C variations in global mean temperature, excluding the Snowball result) is due only to differences in imposed OHT and initial conditions; all runs use identical (realistic) insolation and greenhouse gas levels. The Snowball solutions exist over the entire range of OHT parameters. OHT of several PW under a fully ice-covered ocean is rather unphysical, but it is

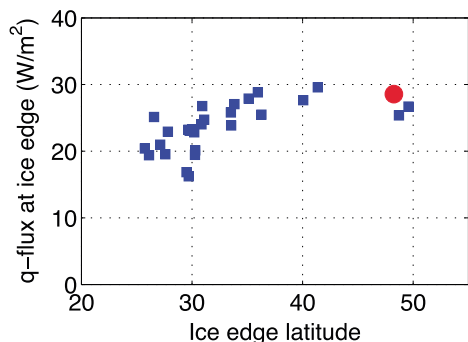


Figure 11. Scatterplot of OHT convergence at the ice edge vs. latitude of ice edge in the slab ocean simulations. Only the runs with a finite ice edge are plotted (blue squares). Corresponding value from the Cold coupled *Aqua* solution from Ferreira *et al.* [2011] plotted in red circle.

into the high latitudes. Rather, it requires sufficient heating of the midlatitude sea surface in order to drive enhanced convection in the midlatitude storm tracks [Rose and Ferreira, 2013].

In the icy regime, the climate is roughly four times more sensitive to variations in OHT (based on the slopes of the equilibrium \bar{T} versus OHT lines). This strong sensitivity is due primarily to the strongly positive albedo feedback associated with changes in sea ice extent [Ferreira *et al.*, 2011; Rose *et al.*, 2013], as well as to the tight coupling of the sea ice edge to the spatial pattern of OHT convergence [Rose and Marshall, 2009; Rose *et al.*, 2013]. In order to examine this coupling in the slab ocean model, we show in Figure 11 a scatterplot of OHT convergence just equatorward of the ice edge in our ensemble of icy states. For ice edges poleward of about 35°, the value is remarkably constant, roughly 25 to 30 W m⁻². Values are somewhat smaller and more highly scattered for colder climates with subtropical ice edges.

There are two distinct regimes of sea ice thickness in these icy states (not shown). At high latitudes where the q-flux is roughly zero, the ice is thick (tens of meters or more). Near the ice margin in the regions where the q-flux is not small (e.g., 20 W m⁻²), the ice is relatively thin (2–3 m). Most of this ice is perennial; seasonal ice extent is very small (of order 1 grid cell). In this thin-ice regime, the OHT convergence (q-flux) heats the base of the ice pack and is balanced by heat conduction through the ice.

In summary, experiments with prescribed OHT in the slab ocean model reveal that the climate is slaved to the size of the ice cap, which is in turn slaved to the shape of the OHT convergence. In the absence of OHT, sea ice advances rapidly into the Snowball state. Sufficiently strong OHT convergence (greater than about 25 W m⁻²) within certain latitude bands presents an energetic barrier to sea ice expansion and permits a stable equilibrium with extensive but finite sea ice cover. Very cold Waterbelt climates with tropical ice edges are possible so long as OHT is sufficiently intense and narrow. The existence of distinctly different Cold and Waterbelt climates in the coupled model is therefore directly linked to the capacity of the ocean circulation to reorganize itself to provide narrow (Waterbelt) versus broad (Cold) meridional scales of OHT.

4. Why Is Sea Ice so Sensitive to OHT?

In this section, we explore some simple ideas about the sensitivity of the sea ice, and by extension the entire climate system, to variations in OHT. We adopt a slight generalization of the well-known diffusive Energy Balance Model (EBM) following North [1975]:

$$K_a \frac{d}{dx} \left((1-x^2) \frac{dT(x)}{dx} \right) - BT(x) = -Q \left\{ \begin{array}{l} a_o \\ a_i \end{array} \right\} (1 + s_2 P_2(x)) + A - F_o(x) \quad \begin{array}{ll} x < x_i & \\ x > x_i & \end{array} \quad (2)$$

Here $x = \sin \phi$ is the independent variable; $T(x)$ is the zonal-mean equilibrium surface temperature in °C; K_a is a coefficient of large-scale heat diffusion for the atmosphere (in W m⁻² °C⁻¹); B is the longwave radiative damping (also in W m⁻² °C⁻¹); $Q (1 + s_2 P_2(x))$ is a reasonable approximation to the observed annual-mean insolation with Q one-quarter of the solar constant in W m⁻², $P_2(x)$ is the second Legendre polynomial, and

permitted in the numerical slab ocean model. In a fully coupled system, the OHT collapses to near-zero once the oceans become fully ice-covered [Ferreira *et al.*, 2011].

Two different regimes are evident in Figure 10 (Warm and Cold climates). In both regimes, global mean temperature increases quasi-linearly with increased OHT. The warm regime ($\bar{T} > 20^\circ$ C in Figure 10) was studied in detail by Rose and Ferreira [2013], who found that OHT plays a key but indirect role in setting \bar{T} by modulating extratropical moist convection and thus controlling the longwave greenhouse trapping in middle to high latitudes. Here we note briefly that the Warm state exists over a broad range of shapes and sizes of OHT, but there are thresholds at which polar ice develops. Once some ice forms, the climate cools rapidly and equilibrates either into a large ice cap or Snowball state. The Warm state does not require OHT

$s_2 = -0.48$; A is the longwave cooling to space associated with a surface at 0°C (in W m^{-2}); x_i is the ice edge latitude (discussed in detail below); a_o and a_i are dimensionless co-albedo values (absorbed fractions) associated respectively with non-icy and icy surfaces. To this standard model, we add a prescribed energy source / sink term $F_o(x)$ representing OHT convergence. This OHT term will be fixed and independent of the climate state in the EBM, as was used in the slab ocean GCM.

4.1. Large Ice Cap Instability: Traditional Analysis

A key dimensionless parameter in the EBM is $\delta = K_a/B$, which measures the efficiency of meridional heat transport in the atmosphere relative to radiative damping. It is well-known that larger δ (i.e., more efficient transport) leads to a less-stable climate in the simple EBM [Held and Suarez, 1974; North et al., 1981]. This parameter is not derived from dynamical principles but rather tuned to reproduce features of the climate of interest. North [1975] finds $\delta = 0.31$ for the observed climate. For our aquaplanet GCM, the warm polar temperatures and weak gradient of the Warm state demand a significantly larger value of δ , with important implications for the number and type of stable equilibria predicted by the EBM, and (as we will show below) their sensitivity to OHT.

Solutions to the EBM are typically presented as graphs of $Q(x_i)$, i.e., the value of solar constant Q required to find the ice edge at a given latitude x_i . The ice edge is typically associated with a specific isotherm $T(x_i) = T_f$ (often taken to be -10°C). Some examples are plotted in Figure 13a for a range of different δ values and $F_o = 0$. These show the multiple equilibrium property of the EBM: for a given Q , there are anywhere from 1 to 5 different x_i that satisfy global energy balance (tracing vertical lines through the graphs). According to the so-called slope-stability theorem [Cahalan and North, 1979], the stability of these equilibria with respect to small perturbations is directly related to the slope of the graph: regions where $dQ/dx_i < 0$ are unstable. In the small δ regime, there is a branch of the solution with positive slope running from the subtropics to the high latitudes. These represent climates with stable finite ice caps, and it is usually supposed that the current climate rests on this branch with a mean ice edge near 70° latitude.

The point we wish to emphasize in this brief review is that at high δ (and without OHT), this stable branch of solutions disappears entirely. Figure 13a shows that for $\delta > 0.4$, the slope is negative everywhere, indicating that a stable climate with a finite-sized ice cap is not possible; the EBM predicts only ice-free and Snowball climates in this regime. As we will show below, the aquaplanet GCM is consistent with the high- δ regime of the EBM, in which stable finite ice caps are possible only in the presence of substantial OHT.

4.2. Ice Thickness and Vertical Heating Distribution

We now add a prescribed pattern of OHT divergence / convergence to the EBM as we have already done in the slab ocean GCM. The convergence of equation (1) yields

$$F_o(x) = -\frac{\Psi}{2\pi R^2} (1-x^2)^{N-1} (1-x^2(2N+1)) \quad (3)$$

One could solve the EBM as above with this prescribed heat source term. However, the model as written here, because it is agnostic about the vertical structure of the heating terms, permits large vertical heat fluxes through the ice in cases where F_o is large and positive at locations where T is cold. This is unphysical, as it ignores the substantial insulating properties of sea ice. Rose and Marshall [2009] side-stepped this problem by enforcing a boundary condition $F_o = 0$ everywhere below the ice in a simple model with interactive OHT. Here we are prescribing a fixed OHT that goes smoothly to zero at the poles, so need to relax the “perfect insulator” assumption invoked by Rose and Marshall [2009] in order to permit some heating under the ice while also respecting the first-order physics of the ocean-sea ice-atmosphere interaction. We therefore invoke a simple thermodynamic model for sea ice thickness H_i . Thorndike [1992] shows in the context of a toy model of Arctic sea ice that the equilibrium thickness of perennial ice is approximately

$$H_i = -\frac{K_i T_i}{F_o} \quad (4)$$

where $K_i = 2 \text{ W m}^{-1} \text{ }^\circ\text{C}^{-1}$ is the thermal conductivity of sea ice, T_i is the temperature of the ice surface, and F_o is the upward heat flux through the ice (balancing the OHT convergence). This situation is sketched in Figure 12, along with the other heat sources and sinks at the ice surface: solar heating, longwave emission to space, and convergence / divergence of atmospheric heat transport. We invoke this balance model in a simple thought experiment to show that ice melts more efficiently when heated from below (i.e., from the ocean) than from above.

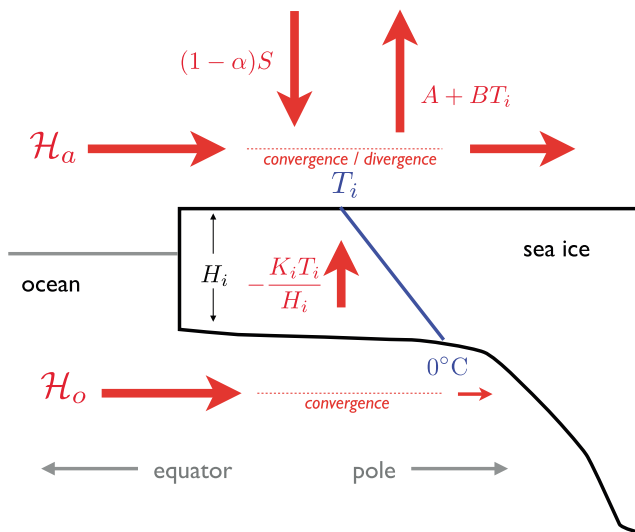


Figure 12. Sketch of the energy budget near the sea ice margin and its relationship to ice thickness. Convergence of OHT under the ice is balanced by upward heat conduction through the ice, which is inversely proportional to ice thickness. Energy balance at the surface involves radiation, convergence of atmospheric heat transport (denoted H_a), and upward heat conduction. The blue line through the ice indicates a linear temperature profile in the ice (which would be expected in a steady state solution in the absence of seasonal heating).

subjected to mechanical breakup and deformation. We are also treating the annual mean energy balance and therefore assuming that ice survives for a sufficient fraction of the year to make an impact on annual mean albedo. From Figure 11, F_o near the ice edge does not exceed 30 W m^{-2} in the GCM. Taking $T_i = -10^\circ\text{C}$ (an annual mean value near the ice edge), we estimate $h_{\min} = 0.67 \text{ m}$. Consistently, in the GCM we find H_i tends to be of order 2–3 m wherever it is experiencing significant heating from below, suggesting that h_{\min} must therefore be somewhat smaller than 2 m. *The ice line is found roughly where the upward flux of heat from the ocean becomes small enough that the ice can achieve sufficient thickness to exert an albedo feedback.* Sensitivity of the ice line to OHT is fundamentally related to the thermodynamic requirements of communicating heat vertically across the air/ice/ocean interface.

A consequence of this assumption is that the ice line cannot be tied to a unique isotherm in the EBM. The ice top temperature T_i must be cold enough to maintain a given upward heat flux. We therefore allow the threshold temperature to depend on OHT convergence at the ice edge:

$$T(x_i) = T_f - \frac{H_{\min} F_o(x_i)}{k_i} = T_f - \eta \frac{F_o(x_i)}{B} \quad (5)$$

where we define $\eta = BH_{\min}/k_i$, an order-1 nondimensional measure of the minimum thickness. Taking $B = 1.5 \text{ W m}^{-2} \text{ }^\circ\text{C}^{-1}$, we estimate $\eta = 0.5$. Equation (5) expresses the notion that for an ice anomaly to exert an albedo feedback, it must have a certain thickness. In the presence of substantial ocean heat flux, it must therefore be very cold and thus strongly damped by longwave radiation to space, which can prevent unstable ice growth at low latitudes where it might otherwise occur without an ocean heat flux. As we will show below, this can lead to *stable low latitude ice edges* in regions of *rapid poleward decrease in heat flux out of the ocean or, equivalently, rapid poleward decrease in OHT convergence*. This is consistent with results from the GCM slab ocean experiments.

4.3. Effects of Prescribed OHT in the Diffusive EBM

Equation (2) (together with (5) and (3)) is a second-order boundary value problem for surface temperature $T(x)$ (subject to no-flux conditions at the equator and pole, and matching conditions at the ice edge). A fully analytical solution is possible, using a slight generalization of the method laid out by North [1975], where the forcing term $F_o(x)$ is expanded in Legendre polynomials. Details are omitted here.

Posit some perturbation that diverts energy from the ice surface (atmosphere) to its base (ocean) and allow the system to re-equilibrate. There is no change in the radiative equilibrium ice-top temperature T_i , but the increased vertical heat conduction requires the ice to thin. While T_i depends only on the column integral energy budget, H_i is sensitive to the vertical distribution of the heating (above and below the ice). This sensitivity stems from the fact that ice is a poor conductor. At equilibrium, then, sea ice thickness is (to first order) controlled by OHT convergence under the ice. If the heat flux through the ice is too large, then ice becomes too thin to be viable.

A key assumption in our modified simple model is the following: for sea ice to have a substantial effect on planetary albedo, it must reach a minimum thickness H_{\min} . Thin ice is not only relatively transparent but also readily

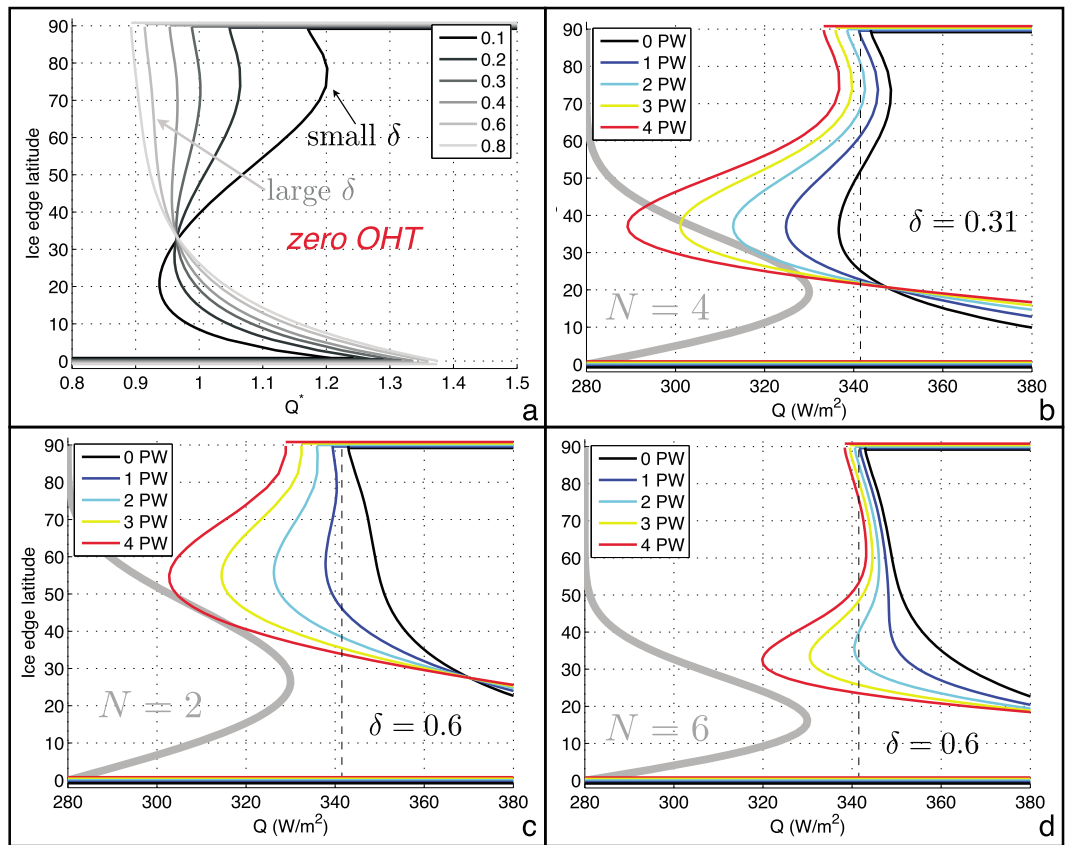


Figure 13. Solutions of the diffusive EBM (2). Plots show ice edge latitude as function of solar constant. (a) solutions with zero OHT ($\Psi = 0$) for various values of the heat transport efficiency parameter δ (plotted in terms of normalized solar constant). (b) effects of OHT (with $N = 4$ and various amplitudes) in the low- δ regime, taking North's estimate of $\delta = 0.31$. (c and d) Effects of OHT in the high- δ regime consistent with the aquaplanet GCM. Parameter values for all solutions are $B = 1.5 \text{ W m}^{-2} \text{ }^{\circ}\text{C}^{-1}$, $A = 215 \text{ W m}^{-2}$, $a_o = 0.7$, $a_i = 0.4$, $T_f = 0^{\circ}\text{C}$, $\eta = 0.5$, except in Figure 13b where we use $B = 1.7 \text{ W m}^{-2} \text{ }^{\circ}\text{C}^{-1}$, $A = 200 \text{ W m}^{-2}$.

Solutions of the EBM are plotted as $Q(x_i)$ in Figure 13. In Figures 13b–13d, we plot $Q(x_i)$ in presence of prescribed OHT. We include the insulating effects of sea ice by setting $\eta = 0.5$ in all cases. Figure 13b represents “Earth-like” parameters: we set $\delta = 0.31$ and the meridional structure of OHT is set to $N = 4$, which captures the shape of the observed subtropical OHT maxima fairly well. We have tuned A such that the ice edge falls near 70° latitude with 2 PW of OHT, roughly the observed maximum in the northern hemisphere. The various colored curves show $Q(x_i)$ for amplitudes on OHT ranging from zero to 4 PW. Stable equilibria exist in these solutions wherever the colored $Q(x_i)$ curves have positive slopes. The vertical dashed lines show the present-day value $Q = 341.5 \text{ W m}^{-2}$.

Figure 13b shows that in the low- δ regime, a reduction in OHT from 2 PW to zero will result in a large but finite equatorward expansion of sea ice down to about 50° (black curve in Figure 13b), rather than a runaway glaciation as we found in the Aquaplanet. (Taking different values of N for the OHT does not alter this prediction qualitatively.) The EBM also predicts that an increase in OHT from 2 to 3 PW at present-day radiative forcing will result in ice-free Earth.

In Figures 13c and 13d, we have tuned the EBM to mimic the Aquaplanet GCM with $\delta = 0.6$, which we will refer to as the “high- δ ” regime. We investigate the effects of OHT with both large and small meridional scale ($N = 2$, Figure 13c and $N = 6$, Figure 13d). These figures show that the size and shape of the OHT exerts a profound effect on the number and type of equilibria predicted by the simple EBM, very much analogous to what we have found in the GCM. As previously noted, in this high- δ regime with zero OHT the EBM is unstable for all finite-sized ice caps (black curves in Figures 13c and 13d). The EBM predicts that a certain minimum value amount of OHT is required to maintain an ice-free climate; otherwise the only possible

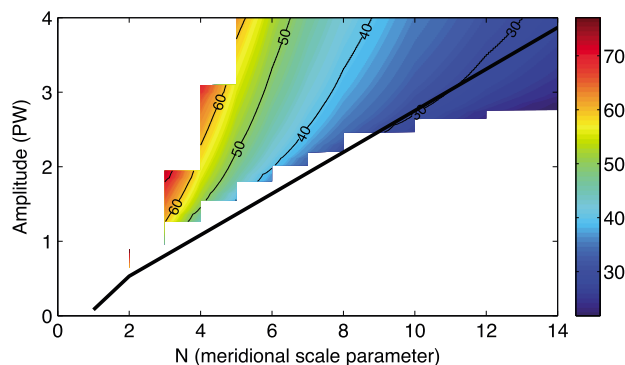


Figure 14. Ice edge latitude as a function of OHT in the EBM, in the high- δ regime fitted to the Aquaplanet GCM. Horizontal axis is the meridional scale parameter N (scale decreasing with larger N); vertical axis is amplitude of imposed OHT in PW. Color contours showing ice edge latitude are plotted wherever a stable solution exists. The thick black line shows the minimum OHT required for an ice-free pole; the warm solutions exists everywhere above this line. Both warm and cold stable solutions exist where color contours are also plotted above this line. In the white space below this line (low amplitude OHT) only the Snowball solution exists.

radiative forcing, depending crucially on the meridional scale of OHT. With $N = 2$ (large scale), there are no stable finite ice caps, because the warming effect of OHT convergence is felt over a very broad range of latitudes. (The EBM does predict stable ice caps at reduced Q with $N = 2$.) On the other hand, with $N = 6$ (small scale OHT) and sufficiently large amplitude, the EBM predicts the co-existence of a stable large ice cap state and the ice-free state. Within this rather narrow range of the parameter space, Figure 13d shows that the ice edge may vary between about 35° and 55° latitude depending on the OHT amplitude.

Figure 14 summarizes the effects of OHT on the ice edge and multiple equilibria in the EBM at present-day radiative forcing ($Q = 341.5 \text{ W m}^{-2}$). The thick black line shows the minimum OHT amplitude required to maintain an ice-free pole (plotted as a function of the meridional scale parameter N); warm ice-free climates are possible everywhere above this line. The color contours show the latitude of the ice edge x_i , wherever a stable icy solution exists. Both warm and cold stable solutions exist wherever color contours are plotted above the black line. In the white space below the black line, only the Snowball climate is possible. This figure shows that multiple equilibria exist across a wide range of possible shapes and sizes of OHT. Stable large ice caps (including ice edges reaching into the tropics) are made possible by high-amplitude, small-scale OHT.

Figures 13 and 14 show that the GCM is largely consistent with the high- δ regime of the EBM, in which stable ice margins cannot exist in the absence of OHT. δ is the ratio of diffusive transport to local LW radiative damping. It is possible that our GCM overestimates δ due to its crude parameterizations of water vapor and cloud feedbacks. The slope of $Q(x_i)$, and thus, the transition from stable to unstable regimes scales as the product $\delta\Delta\alpha$, where $\Delta\alpha = \alpha_o - \alpha_i$ is the albedo contrast between icy and nonicy regions (see next section, and also Roe and Baker [2010]). We have set $\Delta\alpha = 0.3$ throughout these calculations. This provides a good fit to the GCM but implies a relatively strong positive albedo feedback. $\Delta\alpha$ is probably larger for aquaplanets than Earth-like planets due to the high surface albedo contrast between sea ice and open water. Thus, aquaplanets may be systematically less stable than Earth-like planets in the absence of OHT, and our aquaplanet simulations may correspondingly over-emphasize the critical importance of OHT in stabilizing the sea ice margins. On the other hand, the physical link between large ice caps and intense, meridionally narrow bands of tropical OHT is probably robust and not specific to aquaplanet boundary conditions. The EBM shows that such an OHT pattern should play a strong stabilizing role on large ice caps over a wide range of parameter regimes.

4.4. Stability of the Waterbelt: An EBM Analysis

A stable Waterbelt must have a sequence of processes that restore equilibrium following some perturbation. The fact that Waterbelts have been found in both the uncoupled slab ocean GCM and the EBM strongly

equilibrium is the Snowball state. This is precisely what was found in the slab ocean GCM with zero q-flux (c.f. Figure 9). The fact that the ice grows unstably to the equator once the remote polar warming effect of OHT is removed can be attributed to the fact that the Aquaplanet GCM lies in the high- δ regime. The absence of stable moderately-sized ice caps has been noted in previous studies with aquaplanet GCMs without OHT [e.g., Abbot et al., 2011], suggesting that other aquaplanet models also inhabit the high- δ regime.

The $Q(x_i)$ curves in Figures 13c and 13d bulge out toward smaller Q over a range of latitudes set by N . In fact the largest effects are found at the latitudes where OHT convergence decreases poleward. These figures show two qualitatively different ice regimes at present-day

suggests that the essential physics of the stabilization mechanism does NOT depend on an active feedback between the ocean circulation and the rest of the climate system. Coupled atmosphere-ocean-ice processes are essential for the reorganization of the winds and ocean thermal structure to permit different shapes and magnitudes of OHT (e.g., to permit both Cold and Waterbelt climates in the same model), but the behavior of the system near equilibrium ought to be relatively insensitive to this coupling. We therefore analyze small perturbations to the EBM with fixed OHT in order to develop some insight into the stabilization mechanism.

Consider a perturbation $T(x, t) = T'(x, t) + \tilde{T}(x)$ (where primes indicate perturbations and tildes represent equilibrium). To simplify the analysis, we will restrict ourselves to the case of a globally uniform perturbation. The perturbed ice edge is $x_i(t) = x'_i(t) + \tilde{x}_i$. The temperature evolves according to

$$C \frac{dT'}{dt} = \Delta a S(\tilde{x}_i) x'_i(t) - BT'(t) \quad (6)$$

where C is some effective heat capacity and $S(\tilde{x}_i) = Q(1 + s_2 P_2(\tilde{x}_i))$ is the insolation at the equilibrium ice edge. Using equation (5) to relate perturbed ice area and temperature gives

$$T'(t) = -x'_i(t) \left(\frac{d\tilde{T}}{dx} + \frac{\eta}{B} \frac{dF_o}{dx} \right) \Big|_{\tilde{x}_i} \quad (7)$$

where the derivative of F_o arises from considering the ice thickness at a small distance x'_i from the equilibrium ice edge. Plugging this into equation (6) gives an equation for the evolution of the perturbed ice edge

$$C \frac{d}{dt} (\ln x'_i) = -B - \frac{\Delta a S(\tilde{x}_i)}{\left(\frac{d\tilde{T}}{dx} + \frac{\eta}{B} \frac{dF_o}{dx} \right) \Big|_{\tilde{x}_i}} \quad (8)$$

The perturbation will relax toward equilibrium if the RHS is negative. A stability condition on the equilibrium temperature profile near the ice edge is thus (dropping tildes)

$$\Delta a S(x_i) < - \left(B \frac{dT}{dx} + \eta \frac{dF_o}{dx} \right) \Big|_{x_i} \quad (9)$$

Equation (9) expresses the competition between the negative longwave feedback and the positive ice albedo feedback. In the traditional EBM without OHT ($F_o = 0$), factors that destabilize the model and give rise to large ice cap instability include large albedo contrasts, weak longwave damping, and flatter surface temperature gradient near the ice edge (which sets the areal extent of the ice perturbation for a given temperature change). The destabilizing effect of atmospheric heat transport is included implicitly through flattening of the temperature gradient [Roe and Baker, 2010]. Instability becomes increasingly more likely toward the equator as S increases and $-\frac{dT}{dx}$ decreases. Large ice cap instability is a nearly unavoidable consequence of the spherical geometry of the planet.

Equation (9) also states that the oceans stabilize against albedo feedback wherever the OHT convergence decreases poleward, $dF_o/dx < 1$. Equivalently, the OHT must be concave up as a function of sine(latitude). This effect is scaled by the minimum thickness parameter and is a consequence of the thermodynamic coupling of ice thickness to vertical heat flux.

We can now posit a Waterbelt restoring mechanism. Suppose the ocean delivers heat to a certain subtropical latitude belt; the ice edge rests just poleward of this band of heating. The ice thickness increases rapidly poleward of the ice edge, and the surface temperature decreases rapidly. Under a global cooling, there will be a small tendency for ice to advance equatorward. However, the band of strong surface heat flux prevents thick ice from forming. Thus, the positive albedo feedback is weak, radiative damping rules, and the planet warms back to equilibrium. On the other hand, under a global perturbation warming, the ice edge will retreat poleward. But because of the rapid drop-off in OHT convergence and the consequent rapid drop-off in surface temperatures, the area of newly exposed open ocean remains small. Thus, again the positive albedo feedback is weak and radiative damping drives the climate back to equilibrium. The stabilizing mechanism thus relies on a rapid poleward decrease in OHT convergence.

5. Discussion and Conclusions

We have shown that a fully coupled atmosphere-ocean-sea ice GCM supports four distinct stable equilibrium climate states. The four states (Warm, Cold, Waterbelt, and Snowball) span essentially the entire range of past Earth climates, yet are all consistent with present-day insolation and atmospheric composition. The Waterbelt state, which is the principal new finding of this work, extends the work of *Ferreira et al.* [2011] and *Rose et al.* [2013]. To the author's knowledge, no previous work has reported the existence of four stable states in any model of the global climate system, nor has a Waterbelt-like state been shown to be consistent with present-day radiative forcing.

The lack of simple model analogs for the four stable states is notable. The classical EBM can support no more than three stable states. Here we have used two reduced-complexity models—the slab ocean GCM and the diffusive EBM—to quantify the role of spatial structure of OHT in the stabilization of the Waterbelt state. We showed that these uncoupled models support a continuum of stable ice edges for a fixed radiative forcing, including states analogous to both the Cold and Waterbelt states of the fully coupled model. The quantization of this continuum into two distinct climate regimes in the fully coupled system is a result of the active feedback between ice extent, wind stress, and ocean circulation. The physical mechanism appears to rely on robust first-order features of the climate system, e.g., a pattern of surface wind stresses set by baroclinic instability in the atmosphere, and wind-driven subtropical overturning cells. The same mechanism is found to operate in two different configurations of the model with rather different constraints on the ocean circulation (*Aqua* and *Ridge*), suggesting that the results are not beholden to the detailed geometry of the boundary conditions. Should we therefore expect that analogous results could be found in many, perhaps most, coupled GCMs? Or is the existence of four stable states (including a stable Waterbelt at present-day radiative forcing) a pathological case associated with shortcomings of this model (e.g., coarse resolution, highly parameterized moist physics, highly idealized ocean basin configurations, complete absence of land surfaces)? This is unclear at present. *Voigt and Abbot* [2012] found Waterbelt climates with OHT convergence at the ice margin in another coupled GCM, but the heating rates were much weaker than found in this study and (consistent with the arguments in section 4.4 above) did not seem to play a key stabilizing role.

Much previous modeling work on colder climates and the approach to Snowball Earth has used either fixed OHT or fixed wind stress. Such models do not have the necessary coupled interactions to represent the Waterbelt stabilization mechanism described here. On the other hand, studies that have simulated Waterbelt-type climates with fully coupled GCMs [e.g., *Poulsen et al.*, 2001; *Poulsen and Jacob*, 2004; *Yang et al.*, 2012b, 2012c; *Voigt and Abbot*, 2012] have typically employed substantially reduced insolation and CO₂ to simulate Neoproterozoic conditions. Testing for the presence of multiple equilibria and hysteresis was outside the scope of the earliest studies. Such tests are numerically expensive, as they require relatively large numbers of exploratory multimillennial scale integrations of the coupled model (due to the long equilibration time of the deep ocean). Our relatively simplified GCM occupies a unique spot in the climate model hierarchy. It is relatively fast and inexpensive, while the atmosphere and ocean remain fully (physically) coupled through interactive, conservative exchanges of energy, water, and momentum.

One exception is the study by *Yang et al.* [2012a], who reported multiple equilibria in the fully coupled CCSM3 model (their Figure 16). While the authors state that their results are "consistent with EBM-based analyses," in fact they show the coexistence of multiple stable ice edges (large and small ice caps), which are never found in the traditional EBM [*Rose and Marshall*, 2009]. The ocean dynamics are clearly playing an important role in the maintenance of the multiple states in their simulations. Though not the main focus of their study, *Yang et al.* [2012b] describe equatorward contraction of winds and ocean overturning in a Waterbelt-like simulation that is very suggestive of the physics described in this study. On the other hand, a follow-up study with the higher-resolution CCSM4 model [*Yang et al.*, 2012c] did not find multiple states. Multiple states were also explicitly searched for, but not found in, several configurations of the coupled ECHAM5/MPI-OM model [*Voigt and Marotzke*, 2010; *Voigt et al.*, 2011; *Voigt and Abbot*, 2012].

Abbot et al. [2011] discussed a completely different mechanism for stable low-latitude ice edges that can also give rise to hysteresis and multiple states in some models. In the so-called "Jormungand" mechanism, tropical sea ice edges are stabilized by the relatively low albedo of bare (snow-free) sea ice. Bare ice may arise when the sea ice encroaches on the zones of net evaporation / sublimation associated with the descending branch of the atmospheric Hadley circulation. As discussed by *Abbot et al.* [2011] and *Voigt and*

Abbot [2012], this mechanism is sensitive to the model's sea ice albedo scheme, and is not found in models that do not properly represent the albedo contrast between snow and bare ice. Abbot *et al.* [2011] studied this mechanism in an aquaplanet slab ocean GCM with zero OHT and reduced insolation relative to present day.

Our GCM does keep track of snow on sea ice. The albedo of thin bare ice is prescribed as 0.25 in *Ridge* and asymptotes to a maximum value of 0.6 for thick ice, with an exponential scale of 0.25 m, while the albedo of fresh cold snow is 0.8 [Ferreira *et al.*, 2011]. However, the Jormungand mechanism plays no role at all in the stable Waterbelt state described in this paper. The sea ice in our Waterbelt remains snow-covered at all times, and (unlike Abbot *et al.* [2011]) the ice extent has essentially zero seasonal cycle. The equatorward contraction of the atmospheric circulation, which (through its effects on ocean circulation) is a key player in the stabilization mechanism, also results in an equatorward shift of the zones of net evaporation. Thus, in our simulations, the coupled atmosphere-ocean circulation effectively prevents the Jormungand mechanism from operating. These are two completely distinct mechanisms producing a hysteresis for a low-latitude ice edge. There is also essentially no overlap in the two climate states, since we have found Waterbelt climates with ice lines between 21 and 30°, while the Jormungand state has only been found with ice lines between 10 and 20° [Abbot *et al.*, 2011]. It is possible that both mechanisms could operate simultaneously in some models (e.g., perhaps in the work of Yang *et al.* [2012a]) as well as in nature and thereby extend the stable range of the Waterbelt even further. On the other hand, it is not a given that the transition from a stable Waterbelt to warmer climate states necessarily involves a hysteresis. An example of this has been shown recently in the fully coupled ECHAM5/MPI-OM model by Voigt and Abbot [2012].

Voigt and Abbot [2012] also argue that sea ice dynamics play a crucial destabilizing role for low-latitude ice edges—the stable Waterbelt climate is only found in versions of their model in which ice dynamics have been disabled. Our GCM includes only a very simple parameterization of ice transport (diffusion of thickness), and we showed in Figure 7 that the Waterbelt ice line is indeed sensitive to the diffusion coefficient. Diffusive ice thickness tendencies are of order 0.3 cm/day at the ice edge in our reference Waterbelt simulation. Comparing to previous simulations of low-latitude ice states, this is closer to the weak ice dynamics in CCSM3 [Yang *et al.*, 2012a] than to the strong ice dynamics in ECHAM5/MPI-OM [Voigt and Abbot, 2012]. This is a potentially important caveat to our results. It is possible that a more physically complete model of ice dynamics would have a less stable Waterbelt than we have found. On the other hand, many GCMs (including that employed by Voigt and Abbot [2012]) limit the maximum ice thickness under about 10 m for numerical (not physical) reasons. Our GCM has no such artificial limit due to its use of the rescaled vertical coordinate in the ocean model. Equilibrium sea ice thickness exceeds 10 m everywhere across the extratropics in our Waterbelt simulations and in fact reaches 60 m near the poles (though this number is also sensitive to ice diffusivity). How the artificial thickness limits present in most GCMs bias the dynamics of cold climates has never been studied, to the author's knowledge. Much work remains as we explore these less familiar corners of the solution space of our climate models.

Is the Waterbelt a viable alternative to the Hard Snowball for Neoproterozoic glaciations? We can make some qualitative comments despite the many shortcomings of the model used in this study. There is permanent sea ice at the equator in *Ridge*, over a few grid cells on the eastern side of the basin. Here the wind-driven upwelling sustains an SST minimum and the mechanically driven OHT carries energy poleward and up-gradient, a factor missing from models with parameterized diffusive heat transport. As a first guess about the viability of an equatorial ice sheet, we examine the simulated equatorial land snow accumulation on the single zero-elevation land cell comprising the Ridge itself. Permanent year-round snow cover is found at the coldest end of the Waterbelt regime in Figure 7 (ice edge at 21°), though not for our reference case at 1352 m^{-2} . This is roughly consistent with Rodehacke *et al.* [2013], who found equatorial glaciations unlikely with sea ice edges poleward of 20°. Thus, we cannot yet rule out the possibility of a Waterbelt ocean with equatorial glaciation. Further study of Waterbelt climates with explicit Neoproterozoic boundary conditions would be helpful to better constrain this question.

In summary, we offer the following conclusions:

1. A fully coupled atmosphere-ocean-sea ice GCM has four stable states ranging from 100% to 0% ice cover. All four states are found for present-day climate forcing and with two different ocean basin geometries.

2. There is a significant hysteresis associated with the stable Waterbelt state (subtropical sea ice edge, 50 to 64% ice cover, open tropical ocean). It is found over a 47 W m^{-2} range of solar constant, roughly equivalent to a $4 \times \text{CO}_2$ range.
3. The Waterbelt is stabilized by OHT convergence at the ice edges, which are maintained by shallow overturning cells driven by equatorward-shifted global wind systems. This wind shift is tied to the baroclinicity associated with the ice edge. Thus, the Waterbelt depends on a three-way coupled wind-ocean-ice feedback.
4. Models with prescribed (uncoupled) OHT exhibit a continuum of possible cold climates, in which both the ice extent and global mean temperature are slaved to the spatial pattern of OHT (which tends to stabilize the climate system against positive albedo feedback wherever its convergence decreases poleward).
5. The subtropical wind-driven ocean circulation that stabilizes the Waterbelt represents a significant energetic barrier to Hard Snowball initiation. With cold equatorial temperatures and a significant hysteresis, it also offers a potential alternative scenario for Neoproterozoic glaciation. (This is the same argument made by Abbot *et al.* [2011] but on the basis of a completely different physical mechanism).
6. Scenarios for Snowball Earth initiation and deglaciation need to be studied and quantified in fully coupled models. The numerical representation of ice thickness and ice dynamics in Waterbelt climates should be examined more carefully.

Acknowledgments

This work spanned several years. Important aspects were developed while B. R. was at the Massachusetts Institute of Technology and the University of Washington. B. R. thanks John Marshall, David Ferreira, David Battisti, Cecilia Bitz, and Ian Eisenman for numerous inspiring discussions; Aiko Voigt, Dorian Abbot, and Eli Tziperman for their thoughtful reviews; and the editor Steven Ghan. B. R. received funding from a NOAA Climate Climate and Global Change Postdoctoral Fellowship, administered by the University Corporation for Atmospheric Research. Configuration files for the MITgcm are available from the author on request.

References

- Abbot, D. S., A. Voigt, and D. Koll (2011), The Jormungand global climate state and implications for Neoproterozoic glaciations, *J. Geophys. Res.*, **116**, D18103, doi:10.1029/2011JD015927.
- Adcroft, A., and J.-M. Campin (2004), Rescaled height coordinates for accurate representation of free-surface flows in ocean circulation models, *Ocean Model.*, **7**, 269–284, doi:10.1016/j.ocemod.2003.09.003.
- Andrews, T., J. M. Gregory, M. J. Webb, and K. E. Taylor (2012), Forcing, feedbacks and climate sensitivity in CMIP5 coupled atmosphere-ocean climate models, *Geophys. Res. Lett.*, **39**, L09712, doi:10.1029/2012GL051607.
- Ashkenazy, Y., H. Gildor, M. Losch, F. A. Macdonald, D. P. Schrag, and E. Tziperman (2013), Dynamics of a Snowball Earth ocean, *Nature*, **495**, 90–93, doi:10.1038/nature11894.
- Budyko, M. (1969), The effect of solar radiation variations on the climate of the earth, *Tellus*, **21**, 611–619.
- Cahalan, R. F., and G. R. North (1979), A stability theorem for energy-balance climate models, *J. Atmos. Sci.*, **36**, 1178–1188.
- Campbell, A. J., E. D. Waddington, and S. G. Warren (2011), Refugium for surface life on Snowball Earth in a nearly-enclosed sea? A first simple model for sea-glacier invasion, *Geophys. Res. Lett.*, **38**, L19502, doi:10.1029/2011GL048846.
- Campin, J.-M., J. Marshall, and D. Ferreira (2008), Sea ice-ocean coupling using a rescaled vertical coordinate z^* , *Ocean Model.*, **24**, 1–14, doi:10.1016/j.ocemod.2008.05.005.
- Donnadieu, Y., G. Ramstein, F. Fluteau, D. Roche, and A. Ganopolski (2004), The impact of atmospheric and oceanic heat transports on the sea-ice-albedo instability during the Neoproterozoic, *Clim. Dyn.*, **22**, 293–306, doi:10.1007/s00382-003-0378-5.
- Ewing, R. C., I. Eisenman, M. P. Lamb, L. Poppick, A. C. Malof, and W. W. Fischer (2014), New constraints on equatorial temperatures during a Late Neoproterozoic snowball Earth glaciation, *Earth Planet. Sci. Lett.*, **406**, 110–122, doi:10.1016/j.epsl.2014.09.017.
- Ferreira, D., J. Marshall, and B. E. J. Rose (2011), Climate determinism revisited: Multiple equilibria in a complex climate model, *J. Clim.*, **24**, 992–1012.
- Gent, P., and J. C. McWilliams (1990), Isopycnal mixing in ocean circulation models, *J. Phys. Oceanogr.*, **20**, 150–155.
- Held, I. M., and M. J. Suarez (1974), Simple albedo feedback models of the icecaps, *Tellus*, **26**, 613–629.
- Hoffman, P. F., A. J. Kaufman, G. P. Halverson, and D. P. Schrag (1998), A Neoproterozoic Snowball Earth, *Science*, **281**, 1342–1346.
- Hyde, W. T., T. J. Crowley, S. K. Baum, and W. R. Peltier (2000), Neoproterozoic ‘Snowball Earth’ simulations with a coupled climate/ice-sheet model, *Nature*, **405**, 425–429.
- Jackett, D. R., and T. J. McDougall (1995), Minimal adjustment of hydrographic profiles to achieve static stability, *J. Atmos. Oceanic Technol.*, **12**, 381–389.
- Kirschvink, J. (1992), Late Proterozoic low-latitude global glaciation: The Snowball Earth, in *The Proterozoic Biosphere*, edited by J. Kirschvink, pp. 51–52, Cambridge Univ. Press, Cambridge, U. K.
- Klinger, B. A., and J. Marotzke (2000), Meridional heat transport by the subtropical cell, *J. Phys. Oceanogr.*, **30**, 696–705.
- Klinger, B. A., J. Marshall, and U. Send (1996), Representation of convective plumes by vertical adjustment, *J. Geophys. Res.*, **101**, 18,175–18,182, doi:10.1029/96JC00861.
- Marotzke, J., and M. Botzet (2007), Present-day and ice-covered equilibrium states in a comprehensive climate model, *Geophys. Res. Lett.*, **34**, L16704, doi:10.1029/2006GL028880.
- Marshall, J., A. Adcroft, J.-M. Campin, C. Hill, and A. White (2004), Atmosphere-ocean modeling exploiting fluid isomorphisms, *Mon. Weather. Rev.*, **132**, 2882–2894.
- Marshall, J. C., A. Adcroft, C. Hill, L. Perelman, and C. Heisey (1997), A finite-volume, incompressible Navier Stokes model for studies of the ocean on parallel computers, *J. Geophys. Res.*, **102**, 5753–5766.
- McKay, C. P. (2000), Thickness of tropical ice and photosynthesis on a Snowball Earth, *Geophys. Res. Lett.*, **27**, 2153–2156.
- Molteni, F. (2003), Atmospheric simulations using a GCM with simplified physical parameterizations. I: Model climatology and variability in multi-decadal experiments, *Clim. Dyn.*, **20**, 175–191.
- North, G. R. (1975), Analytical solution to a simple climate model with diffusive heat transport, *J. Atmos. Sci.*, **32**, 1301–1307.
- North, G. R., R. F. Cahalan, and J. A. Coakley (1981), Energy balance climate models, *Rev. Geophys. Space Phys.*, **19**, 91–121.
- Pierrehumbert, R. T., D. S. Abbot, A. Voigt, and D. Koll (2011), Climate of the Neoproterozoic, *Annu. Rev. Earth Planet. Sci.*, **39**, 417–460.
- Pollard, D., and J. F. Kasting (2005), Snowball Earth: A thin-ice solution with flowing sea glaciers, *J. Geophys. Res.*, **110**, C07010, doi:10.1029/2004JC002525.
- Poulsen, C., and R. Jacob (2004), Factors that inhibit Snowball Earth simulation, *Paleoceanography*, **19**, PA4021, doi:10.1029/2004PA001056.

- Poulsen, C. J., R. T. Pierrehumbert, and R. L. Jacob (2001), Impact of ocean dynamics on the simulation of the neoproterozoic "Snowball Earth", *Geophys. Res. Lett.*, 28, 1575–1578, doi:10.1029/2000GL012058.
- Redi, M. H. (1982), Oceanic isopycnal mixing by coordinate rotation, *J. Phys. Oceanogr.*, 12, 1154–1158.
- Rodehacke, C. B., A. Voigt, F. Ziemen, and D. S. Abbot (2013), An open ocean region in Neoproterozoic glaciations would have to be narrow to allow equatorial ice sheets, *Geophys. Res. Lett.*, 40, 5503–5507, doi:10.1002/2013GL057582.
- Roe, G. H., and M. B. Baker (2010), Notes on a catastrophe: A feedback analysis of Snowball Earth, *J. Clim.*, 23, 4694–4703.
- Rose, B. E. J., and D. Ferreira (2013), Ocean heat transport and water vapor greenhouse in a warm equitable climate: A new look at the low gradient paradox, *J. Clim.*, 26, 2117–2136, doi:10.1175/JCLI-D-11-00547.1.
- Rose, B. E. J., and J. Marshall (2009), Ocean heat transport, sea ice, and multiple climate states: Insights from energy balance models, *J. Atmos. Sci.*, 66, 2828–2843.
- Rose, B. E. J., D. Ferreira, and J. Marshall (2013), The role of oceans and sea ice in abrupt transitions between multiple climate states, *J. Clim.*, 26, 2862–2879, doi:10.1175/JCLI-D-12-00175.1.
- Sellers, W. D. (1969), A global climatic model based on the energy balance of the earth-atmosphere system, *J. Appl. Meteorol.*, 8, 392–400.
- Thorndike, A. (1992), A toy model linking atmospheric thermal radiation and sea-ice growth, *J. Geophys. Res.*, 97, 9401–9410.
- Trenberth, K., J. Olson, and W. Large (1989), A global ocean wind stress climatology based on ECMWF analyses, *Tech. Rep. NCAR/TN-338+STR*, Natl. Center Atmos. Res., Boulder, Colo.
- Trenberth, K. E., and J. M. Caron (2001), Estimates of meridional atmosphere and ocean heat transports, *J. Clim.*, 14, 3433–3443.
- Tziperman, E., D. S. Abbot, Y. Ashkenazy, H. Gildor, D. Pollard, C. G. Schoof, and D. P. Schrag (2012), Continental constriction and oceanic ice-cover thickness in a Snowball-Earth scenario, *J. Geophys. Res.*, 117, C05016, doi:10.1029/2011JC007730.
- Voigt, A., and D. S. Abbot (2012), Sea-ice dynamics strongly promote snowball earth initiation and destabilize tropical sea-ice margins, *Clim. Past*, 8, 2079–2092, doi:10.5194/cp-8-2079-2012.
- Voigt, A., and J. Marotzke (2010), The transition from the present-day climate to a modern Snowball Earth, *Clim. Dyn.*, 35, 887–905, doi:10.1007/s00382-009-0633-5.
- Voigt, A., D. S. Abbot, R. T. Pierrehumbert, and J. Marotzke (2011), Initiation of a Marinoan Snowball Earth in a state-of-the-art atmosphere-ocean general circulation model, *Clim. Past*, 7, 249–263.
- Winton, M. (2000), A reformulated three-layer sea ice model, *J. Atmos. Oceanic Technol.*, 17, 525–531.
- Yang, J., W. R. Peltier, and Y. Hu (2012a), The initiation of modern "soft Snowball" and "hard Snowball" climates in CCSM3. Part I: The influence of solar luminosity, CO₂ concentration and the sea ice/snow albedo parameterization, *J. Clim.*, 25, 2711–2736.
- Yang, J., W. R. Peltier, and Y. Hu (2012b), The initiation of modern "soft Snowball" and "hard Snowball" climates in CCSM3. Part II: Climate dynamic feedbacks, *J. Clim.*, 25, 2737–2754.
- Yang, J., W. R. Peltier, and Y. Hu (2012c), The initiation of modern soft and hard Snowball Earth climates in CCSM4, *Clim. Past*, 8, 907–918.